

# Journal of Materials Chemistry A

Accepted Manuscript



This is an *Accepted Manuscript*, which has been through the Royal Society of Chemistry peer review process and has been accepted for publication.

*Accepted Manuscripts* are published online shortly after acceptance, before technical editing, formatting and proof reading. Using this free service, authors can make their results available to the community, in citable form, before we publish the edited article. We will replace this *Accepted Manuscript* with the edited and formatted *Advance Article* as soon as it is available.

You can find more information about *Accepted Manuscripts* in the [Information for Authors](#).

Please note that technical editing may introduce minor changes to the text and/or graphics, which may alter content. The journal's standard [Terms & Conditions](#) and the [Ethical guidelines](#) still apply. In no event shall the Royal Society of Chemistry be held responsible for any errors or omissions in this *Accepted Manuscript* or any consequences arising from the use of any information it contains.

# Sulfur/Carbon Nanocomposite-filled Polyacrylonitrile Nanofibers as Long Life and High Capacity Cathode for Lithium-Sulfur Batteries

Jian Ye, Feng He, Jia Nie, Yuliang Cao, Hanxi Yang, Xiping Ai\*

Received (in XXX, XXX) Xth XXXXXXXXXX 20XX, Accepted Xth XXXXXXXXXX 20XX

DOI: 10.1039/b000000x

Sulfur/carbon (S/C) nanocomposite-filled polyacrylonitrile (PAN) nanofibers (denoted as S/C/PAN) are synthesized as a long life and high capacity cathode material for lithium-sulfur (Li-S) batteries. In the S/C/PAN nanofibers, the sulfurized PAN matrix acts not only as ionic and electronic channels to allow  $\text{Li}^+$  and electrons to arrive at and react with the S/C nanoparticles, but also as a protective barrier to prevent the S/C nanoparticles from contacting with electrolyte, thus avoiding the discharge intermediates of sulfur to dissolve in and react with the organic carbonate electrolyte. Since the redox reaction of sulfur in the nanofibers occurs mostly at the interior S/C interface through a solid state reaction mechanism, the microstructures and electrochemical interfaces in the nanofibers cathode remain stable during repeated cycles. As a consequence, the S/C/PAN cathode demonstrate a high reversible capacity of  $1179 \text{ mA h g}^{-1}$  at a current rate of  $200 \text{ mA g}^{-1}$ , a high Coulombic efficiency of  $\sim 100\%$  after a few cycles, a good rate capability with  $616 \text{ mA h g}^{-1}$  at  $4.0 \text{ A g}^{-1}$  and a long cycling stability with 60% capacity retention over 400 cycles, showing a great prospect for Li-S battery applications.

## Introduction

With the rapid development of advanced portable electronics, zero-emission electric vehicles and renewable power stations, low cost and high capacity batteries are in great demand for widespread electric storage applications.<sup>1-2</sup> In this technology development, lithium-sulfur (Li-S) batteries have attracted particular attention as a promising candidate for next-generation energy-storage devices because of their high theoretical energy density ( $2600 \text{ Wh Kg}^{-1}$ ), wide availability, low cost and non-toxicity of sulfur resources, all of which offer competitive advantages for large scale applications.<sup>3-7</sup>

Despite such significant advantages, realizing a practical Li-S battery is difficult, primarily due to the intrinsic drawbacks of sulfur electrode.<sup>8-12</sup> As is well known, sulfur and its discharge products ( $\text{Li}_2\text{S}_2$  and  $\text{Li}_2\text{S}$ ) are electronically and ionically insulating, which leads to a poor electrochemical utilization of sulfur cathode. Besides, the dissolving and consequent shuttling of lithium polysulfides generated as intermediates during charge-discharge processes in the electrolyte can cause serious capacity fading and low coulombic efficiency. Moreover, the large mechanical stress induced by the volume expansion from sulfur ( $d = 2.03 \text{ g cm}^{-3}$ ) to its discharge product, lithium sulfide ( $\text{Li}_2\text{S}$ ,  $d = 1.66 \text{ g cm}^{-3}$ ), may break the integrity of sulfur cathode, which accelerates, in turn, the capacity fading. Therefore, improving the electronic conductivity, accommodating volume change as well as avoiding the dissolution of polysulfides plays an equal importance to achieve a stable sulfur cathode.

To improve the electrochemical rechargeability of sulfur electrodes, considerable efforts have been made to address these

problems in the past decade. A major strategy is to fabricate nanostructured sulfur/carbon (S/C) composite by impregnating sulfur molecules into the nanopores of conductive carbon matrixes to make them electrochemically active. Various porous carbon materials such as carbon nanotubes and nanofibers,<sup>13-18</sup> micro- or meso-porous carbons,<sup>19-25</sup> porous hollow carbons,<sup>26-29</sup> carbon nanospheres,<sup>20-23,29,30</sup> and grapheme<sup>14,16,31-33</sup> have been extensively investigated as sulfur hosts because of their high electronic conductivity and particularly, abundant pore volume, which provide not only confined channels to restrain the outward diffusion of polysulfide intermediates, but also sufficient void space to accommodate the volumetric expansion of sulfur during cycling. Furthermore, the adsorption properties of porous carbon matrixes are also helpful to trap the dissolved polysulfide anions within the pores and thus to alleviate the shuttling effect. Though these methods could improve the electrochemical utilization and the cycling stability of sulfur electrode considerably, it is still difficult to avoid the diffusion lose of sulfur by the weak physical adsorption between the nonpolar carbon and the highly polar polysulfide anions. Therefore, the shuttling of polysulfides as well as the capacity fading still remains a problem for the S/C composites.

To improve the cycling stability of the S/C composites, a number of additional strategies have been proposed to alleviate the shuttle effect. These include: 1) inserting a barrier layer (mesoporous silica and  $\text{Al}_2\text{O}_3$  or microporous carbon) in-between the cathode and separator to capture polysulfide intermediates;<sup>34-37</sup> 2) tailoring electrolytes to restrain polysulfides dissolution, or replacing the organic electrolytes with ionic liquid electrolytes, polymer and “solvent-in-salt” electrolytes to lower down the

mobility of polysulfides;<sup>38-42</sup> 3) employing  $\text{LiNO}_3$  or  $\text{P}_2\text{S}_5$  as safeguard additives to passivate the Li surface and thus to inhibit the reduction of higher order polysulfide ions on Li anode;<sup>43-44</sup> and 4) encapsulating S/C composite with conductive polymer such as polythiophenes, polypyrrole.<sup>45-47</sup> Nevertheless, in most cases, the discharge capacity of the S/C composites still decay slowly with increasing cycle numbers. To gear the Li-S battery research towards practical applications, more effective strategies, especially those that can greatly depress or even fully eliminate the diffusion loss of the polysulfides are highly desired for developing cycling-stable sulfur cathodes.

A few of previous studies have demonstrated that use of organic carbonate-based electrolytes widely used in current lithium ion batteries can effectively suppress the dissolution loss of the reaction intermediates of sulfur, enabling the sulfur-encapsulated microporous carbon spheres to achieve high coulombic efficiency (approaching 100% after 3 cycles) and excellent cyclability.<sup>20</sup> However, this strategy is difficult to apply for the conventional sulfur cathodes due to the high reactivity of carbonates with polysulfides,<sup>23</sup> which makes sulfur almost entirely inert. To avoid this situation, it seems that the sulfur nanoparticles should be embedded in the interior micropores of the carbon matrixes, so as to reduce the direct contact with the carbonate electrolyte. This is the reason why the well cyclable S/C composites in the carbonate-based electrolytes reported so far are all sulfur-encapsulated microporous carbon spheres.<sup>8,20,23</sup>

Another sulfur electrode compatible with carbonate-based electrolytes reported so far is polyacrylonitrile/sulfur (PAN/S) composites, which are usually obtained by heating a mixture of PAN and sulfur to make PAN cyclized, dehydrogenized and finally sulfurized.<sup>48</sup> Benefiting from the electrical and ionic conductivity of the thus-sulfurized PAN framework, these composites usually demonstrate high sulfur utilization and stable cycleability in the carbonate-based electrolytes. However, the low sulfur content in the PAN/S composites (< 40 wt. %) hinders their battery application.

Enlightened from the structural features of both sulfur-encapsulated microporous carbon spheres and PAN/S composites, here, we proposed a new strategy to develop cycling-stable sulfur electrodes in carbonate-based electrolytes by embedding sulfur/carbon composite nanoparticles into a  $\text{Li}^+$ -conductive polymer matrix, thus preventing the direct contact of sulfur with liquid electrolyte. In such a material,  $\text{Li}^+$  ions and electrons transport through the polymer matrix into the interior of the cathode to react with the embedded sulfur, thus avoiding the dissolution of the intermediates into the bulk electrolyte.

To realize this concept, we prepared S/C composite nanoparticle-filled PAN nanofibers (denoted as S/C/PAN) by a single-nozzle electrospinning technique and subsequent heat-treatment at 280 °C to make PAN sulfurized and therefore conductive. Benefiting from the structural features, the thus-prepared C/S/PAN nanofiber cathode has good compatibility with the conventional carbonate-based electrolytes and exhibits high Coulombic efficiency, long cycle life and good rate capability, showing a great prospect for battery applications.

## Experimental

### Preparation of S/C composite

A commercial microporous carbon, BP2000 (Black Pearls 2000, Cabot Corporation), with an average particle size of 12 nm, surface area of about  $1300 \text{ m}^2 \text{ g}^{-1}$  and average pore size of 0.7 nm, was adopted as conductive matrix to fabricate C/S composite. The C/S composite was prepared by a conventional melt-diffusion method. First, BP2000 was mixed with sublimed sulfur at a weight ratio of 1:4 in a planetary mill (QM-1SP04, Nanjing, China), then, the mixture was sealed in a stainless steel vessel and heated at 155 °C for 6 h. After cooling down, the obtained sample was ground by ball-milling at a rotation speed of 200 rpm for 6 h to obtain S/C composite.

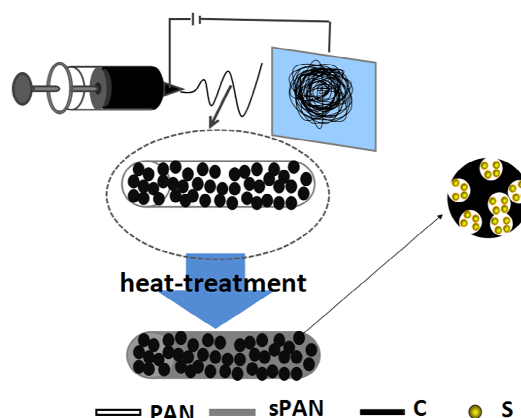
### Preparation of electrospinning solution

PAN with a molecular weight of 150 000 was purchased from Sigma-Aldrich. N, N-dimethyl formamide (DMF) was used as the solvent of PAN and dispersant of S/C composite. Spinning solution was obtained by adding the S/C composite to 8 wt. % PAN/DMF solution and then fine-grinding in a Mini-Mill Pulverisette 23 (Fritsch, Germany) with an oscillation frequency of 35 Hz for at least 3–4 h. The mass ratio of S/C composite to PAN was designed as 5:2 in the spinning solution.

### Electrospinning and heat-treatment

The synthetic processes of the S/C/PAN nanofibers are schematically illustrated in scheme 1. The spinning solution was contained in a syringe with a stainless steel nozzle (0.47 mm internal diameter). The nozzle was connected to a high-voltage regulated DC power supply (Model DW-N503-1ACDF, Tianjin, China). A constant volume flow rate was maintained via a syringe-type infusion pump (Model LSP01-1A, Shanghai, China). An applied voltage of 16 kV, solution flow rate of  $0.8 \text{ mL h}^{-1}$ , and distance between the nozzle-tip to the aluminium foil collector of 10 cm were found to provide a steady electrospinning operation.

The as-collected nanofibers were heat-treated at an optimized temperature of 280 °C for 3h with a heating rate of  $2 \text{ }^\circ\text{C min}^{-1}$  in a sealed stainless steel autoclave. During this process, PAN polymer chains were cyclized and dehydrogenated by releasing small hydrogen sulfide ( $\text{H}_2\text{S}$ ) molecules, the resulting carbon double bonds were instantly sulfurized by the sulfur on the carbon matrix.<sup>49</sup>



**Scheme 1** Schematic diagram of the preparation process for the C/S/PAN nanofibers.

### Structure characterization

The morphological and structural characteristics of the as-prepared fibers were examined by X-ray diffraction (XRD), scanning electron microscopy (SEM), transmission electron microscopy (TEM) and X-ray photoelectron spectroscopy (XPS). The XRD patterns were recorded with a Shimadzu XRD-6000 (Kyoto, Japan) diffractometer by using a Cu K $\alpha$  target at 40 kV and 30 mA with a scan rate of 4 ° min<sup>-1</sup>. SEM and TEM images were taken with a SUPRA 55VP FESEM microscopy (Zeiss Sigma) operated at 15 kV and a Tecnai G2 F30 microscopy (FEI, Netherland) at an accelerating voltage of 300 kV, respectively. The TEM was coupled with an energy dispersive X-ray spectrometer (EDX) for determining the chemical composition of the samples. XPS was performed on a Thermo Fisher ESCALAB 250 X-ray photo-electron spectroscope using Al K $\alpha$  X-rays (1486.68 eV) as the excitation source under an ultrahigh vacuum. The binding energies were calibrated relative to the C1s peak (284.8 eV). All the high resolution spectra were obtained under constant analyzer energy (CAE) mode with pass energy of 20 eV and step size of 0.05eV. The sulfur content in the composite nanofibers was determined by elemental analysis using a Vario EL III elemental analyzer.

### Electrochemical measurements

All the electrochemical tests were carried out using 2016 coin-type cells with lithium foil as both anode and reference electrode. The cathode was prepared by coating the slurry of the C/S/PAN nanofibers, Ketjen Black conductive additive and carboxymethyl cellulose (CMC) binder in a weight ratio of 70:20:10 in distilled water on aluminum foil and followed by drying at 60 °C in vacuum for 12h. The as-prepared electrode was cut into disks

with a diameter of 1 cm for assembling cells. The cells were assembled in an argon-filled glove box with a microporous membrane (Celgard 2300) as separator. The organic carbonate electrolyte used in this study was 1 M LiPF<sub>6</sub> dissolved in a mixture of propylene carbonate (PC), ethylene carbonate (EC), and diethyl carbonate (DEC) in a volume ratio of 1:4:5, purchased from the Performance Materials Company (Ferro, Suzhou). The galvanostatic charge and discharge tests were performed at a voltage interval of 1.0–3.0 V using a programmable computer-controlled battery charger (CT2001A Land Battery Testing System, Wuhan, China). The specific capacity was calculated on the mass weight of the sulfur in the composite fibers. Cyclic voltammetric measurements were carried out with the coin cells at a scan rate of 0.1 mV s<sup>-1</sup> using a CHI 660c electrochemical workstation (Chen Hua Instruments Co., China).

### Results and Discussion

The C/S/PAN composite nanofibers were prepared by electrospinning the dispersion of S/C composite in a PAN/DMF solution, followed by heat-treatment at 280 °C to make PAN sulfurized. The mass ratio of S/C composite to PAN polymer was 5:2 in the electrospinning solution. The S/C composite was obtained by a melt-diffusion technique to disperse sublimed sulfur in microporous BP2000 matrix at 155 °C. The sulfur content in the S/C composite was 80 wt. %. The morphology and structural features of the as-prepared C/S/PAN fibers were characterized by SEM, TEM and XRD. As revealed by the SEM image in Fig. 1a, the as-prepared fibers have smooth surface and uniform morphology with a diameter in the range of 100–200 nm.

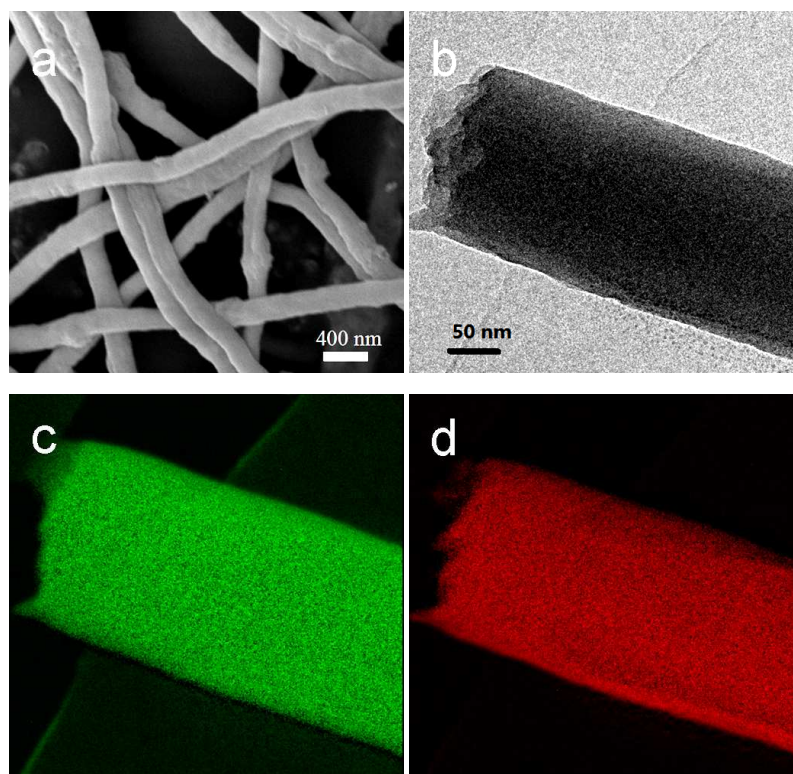


**Fig. 1** SEM image (a); TEM image (b); the corresponding elemental mapping of carbon (c) and sulfur (d) for the as-prepared C/S/PAN nanofibers.

The TEM image in Fig. 1b shows a dense surface of the composite nanofibers without any discernable porosity. Apparently, this structural feature is beneficial to prevent the electrolyte penetrating into the interior space of the fibers and to block off the direct contact of embedded S/C nanoparticles with the bulk electrolyte, so as to avoid the side reaction between the reaction intermediates of sulfur and carbonate solvents, thus enabling the fibrous sulfur electrode compatible with the carbonate-based electrolytes. Nevertheless, the embedded S/C nanoparticles can not be discerned from the TEM image due to their deep encapsulation in the fibrous matrix as well as the very low contrast of the sulfurized PAN and the S/C composite. The corresponding elemental mappings in Fig. 1c and 1d demonstrate a homogeneous distribution of both carbon and sulfur in the composite nanofibers. To further characterize the structure features of the C/S/PAN fibers, the fibers were cut off and the cross-section was viewed by SEM. The SEM image in Fig. S1a reveals that the S/C nanoparticles (strong contrast) were homogeneously dispersed and embedded in the sulfurized PAN matrix (weak contrast). The corresponding elemental mappings in Fig. S1b and 1c also display a homogeneous distribution of both carbon and sulfur over the cross-section, indicating that the sulfur is indeed inside the fiber matrix. The content of sulfur in the nanofibers is determined to be 53% by elemental analysis.

The phase structures of S/C composite and C/S/PAN nanofibers were characterized by X-ray diffraction (XRD) as shown in Fig. 2. The XRD pattern of the pristine S was also displayed for comparison. As observed in Fig. 2, the pristine S exhibits sharp and intense diffraction peaks, indicating its presence in a highly crystalline state. In the case of S/C composite, the peaks belonging to crystalline S<sub>8</sub> phases are still visible, but their intensities are substantially reduced due to the uniform distribution of the sulfur in the BP2000 matrix. After further electrospun with PAN and subsequently heat-treated, the C/S/PAN nanofibers show featureless diffractions with a broad and weak band at  $2\theta \approx 25^\circ$ , characterizing the amorphous structure of carbon and PAN matrix. This suggests that the S/C composite were deeply embedded and well dispersed in the PAN-based nanofibers.

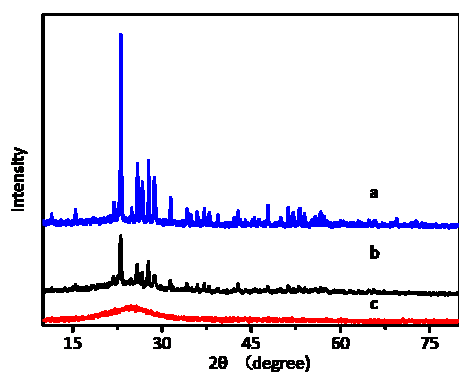


Fig.2 XRD patterns of (a). sublimed sulfur, (b). C/S composite and (c). the as-prepared C/S/PAN nanofibers.

X-ray photoelectron spectroscopy (XPS) was used to further characterize the chemical composition of C/S/PAN nanofibers.

Fig. 3a shows the XPS spectra in the C 1s region. Fitted curves reveal that the C 1S band can be split into three peaks. The main peak at 284.6 eV corresponds to the sp<sup>2</sup>-hybridized carbon.<sup>50</sup> The peak at 285.5 eV can be partially ascribed to the C-S bonds,<sup>50</sup> suggesting successful sulfurization of PAN in the heat-treatment process. The minor peak centered at 286.6 eV can be attributed to the C-O species formed by carbon oxidation during the sulfurization process. The XPS spectra of the S 2p (Fig. 3b) shows an overlapped band with two shoulder bands. The main peak is virtually composed of two strong peaks at 163.5 eV and 164.7 eV, which have an energy separation of 1.2 eV and an intensity ratio of 2:1, obviously due to S 2p 1/2 and S 2p 3/2 doublet of elemental S.<sup>50</sup> This observation demonstrates that the sulfur in the nanofibers exists dominantly in an elemental state. Nevertheless, the lower binding energy of S 2p 3/2 state (163.5eV) than elemental sulfur (164.0eV) reveals the presence of C-S bond in the nanofibers. The minor peak centered at 168 eV arises from the sulphate species most likely formed by the oxidation of elemental sulfur during the preparation process. The peak at 161.7 eV can be attributed to the adsorbed H<sub>2</sub>S by-product generated in the sulfurization reaction.

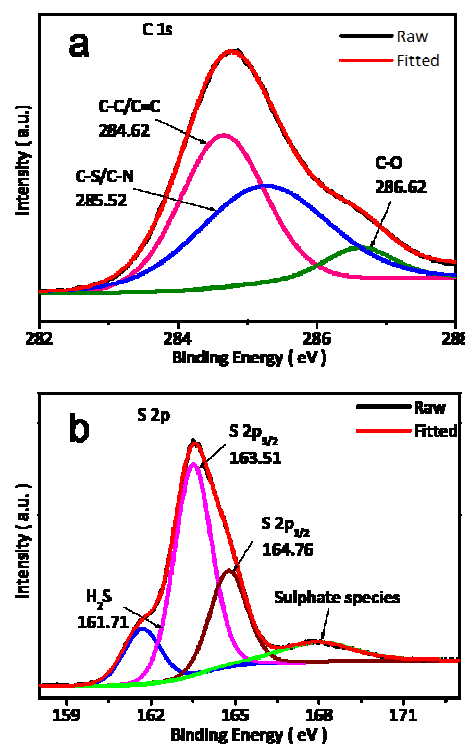
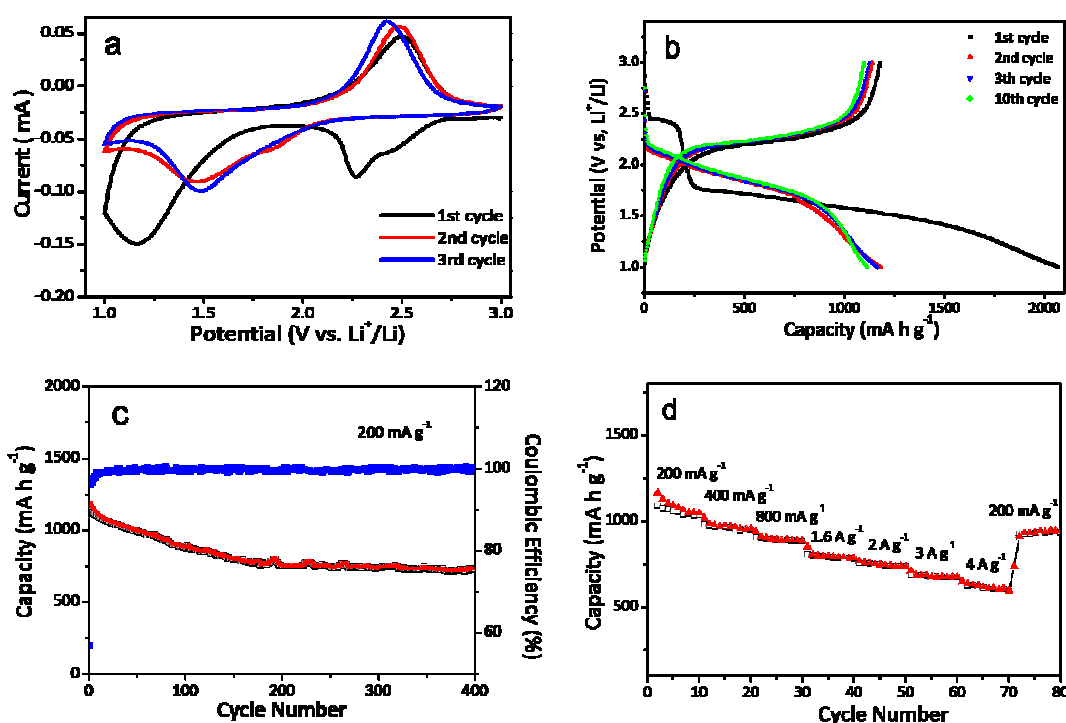


Fig.3 XPS analysis of C/S/PAN nanofibers. (a) C 1s spectrum; (b) S 2p spectrum.

The electrochemical performances of the as-prepared C/S/PAN nanofibers were evaluated as cathode for Li-S batteries in coin cells. The coin cells were assembled with electrolyte of 1 M LiPF<sub>6</sub>/PC-EC-DEC (1:4:5, by vol.). Fig. 4a shows the cyclic voltammograms (CV) of the C/S/PAN nanofiber cathode in carbonate-based electrolyte at a scan rate of 0.1 mV s<sup>-1</sup>. As can be seen, the composite nanofibers exhibit two cathodic peaks in the first cycle: a small one at ~ 2.3 V (vs. Li/Li<sup>+</sup>) and a large one

starting at  $\sim 1.8$  V. The small peak disappears after the first scan, while the onset potential of the large peak shifts to a more positive value of 2.1 V at the subsequent scans. The appearance of the high potential peak demonstrates the existence of a small amount of residual sulfur on the surface region of the nanofibers, which is reduced to form high-order polysulfides in the first cathodic process and reacted with carbonate solvents. The low potential peak arises from the S/C nanoparticles embedded within the sulfurized PAN fibers, where sulfur is reduced, lithiated and finally converted to lithium sulfide ( $\text{Li}_2\text{S}$ ). Nevertheless, the reduction potential of the S/C composite in such PAN-based nanofibers is much lower than the thermodynamic value of sulfur. A possible explanation is that a large mass transfer polarization is needed for driving the  $\text{Li}^+$  ions to pass through the sulfurized

PAN matrix and to arrive at the S/C nanoparticles for sulfur reduction. This is confirmed by the fact that the CV peak of the as-prepared nanofibers resembles very much that of the PAN/S composite in the shape and position.<sup>51</sup> Another question is the positive shift of the reduction peak after the first scan. This phenomenon is most likely caused by the large strain due to the volume expansion of the embedded sulfur in the initial reduction, which requires an additional polarization and therefore produces such a potential hysteresis. For anodic scan, only a single peak appears at  $\sim 2.4$  V, reflecting the oxidation reaction of the reduction product  $\text{Li}_2\text{S}$ . In the following scans, the cathodic and anodic current peaks become almost unchanged in the position and intensity, demonstrating a high cycling stability of the S/C/PAN nanofiber cathode.



**Fig.4** Electrochemical performances of the C/S/PAN nanofiber cathode using the electrolyte of 1 M  $\text{LiPF}_6/\text{PC-EC-DEC}$ : (a) Cyclic voltammograms in the initial three cycles within the voltage range of 1.0 V–3 V (vs.  $\text{Li}^+/\text{Li}$ ) at a scan rate of  $0.1 \text{ mV s}^{-1}$ ; (b) Discharge/charge voltage profiles at a current density of  $200 \text{ mA g}^{-1}$ ; (c) Cycling performance and Coulombic efficiency curves, and (d) Rate capability at various current density from  $200 \text{ mA g}^{-1}$  to  $4.0 \text{ A g}^{-1}$ .

The galvanostatic charge–discharge behaviors of the S/C/PAN nanofibers in carbonate-based electrolyte are shown in Fig. 4b. In accord with the CV curves, the nanofiber cathode displays a two-staged potential profile with a short plateau at a higher potential of 2.4 V and a long plateau at a lower potential of  $\sim 1.7$  V at the first discharge, giving a total discharge capacity of  $2069 \text{ mA h g}^{-1}$ . Since the second cycle, the short plateau at 2.4 V disappears, while the lower plateau at 1.7 V becomes steeper and shifts to 1.8 V with the discharge capacity down to  $1183 \text{ mA h g}^{-1}$  and the Coulombic efficiency up to  $\sim 96\%$ . Apparently, the short plateau at 2.4 V should be attributed to the reduction of residual sulfur, which is produced by the deposition of vaporized sulfur on the outer surface of nanofibers during cooling down after heat-treatment. These residues were reduced to high-order polysulfides

at the first discharge and subsequently deactivated in the subsequent cycles due to the side reaction between polysulfide anions and carbonate solvents, resulting in the disappearance of short plateau at 2.4 V after the first discharge. Along with the lower discharge plateau, the nanofiber electrode shows only a single charge plateau at around 2.2 V. The charge capacities are  $1179 \text{ mA h g}^{-1}$ ,  $1137 \text{ mA h g}^{-1}$  and  $1126 \text{ mA h g}^{-1}$  in the first, second and third cycle, respectively, showing a high reversible capacity of the S/C/PAN nanofiber cathode. Although the reversible capacity is sufficiently high, there still exists a large irreversible capacity of  $\sim 886 \text{ mA h g}^{-1}$  in the first cycle. Except for the part of the irreversible capacity due to the reduction of the surface sulfur at 2.4 V, the major part of irreversible capacity ( $\sim 580 \text{ mA h g}^{-1}$ ) delivered at the potential below 1.7 V is

exclusively attributed to the formation of SEI film on the surface of nanofibers. The low Coulombic efficiency (~56%) in the first cycle quickly increases to 96% in the second cycle and to 99% in the third cycle, suggesting that SEI film is rapidly formed in the initial cycles. This SEI film can act as a protective layer to prevent polysulfides from reacting with carbonate-based electrolyte and therefore to improve the cyclability of the nanofiber cathode.

The cycling performance of the S/C/PAN nanofiber cathode in carbonate-based electrolyte is given in Fig. 4c. At a current density of 200 mA g<sup>-1</sup>, the reversible capacity of the nanofiber composite is 1183 mA h g<sup>-1</sup> at the 2nd cycle and gradually decreases to ca. 795 mA h g<sup>-1</sup> over 150 cycles and then maintains stable at subsequent cycles. Even cycled for more than 400 cycles, the nanofiber cathode can still retain a quite high capacity of > 730 mA h g<sup>-1</sup>, demonstrating a stable cycling performance. As can also be seen from Fig. 4c, after the first three cycles, the Coulombic efficiency of the nanofiber composite reaches nearly 100% during extended cycling. The high reversible capacity, long cycle life and high Coulombic efficiency suggest that the sulfurized PAN matrix can effectively confine the S/C composite and stabilize the polysulfide intermediates.

In addition to the high capacity and strong cyclability, the S/C/PAN nanofiber cathode also demonstrates an excellent rate capability. As shown in Fig. 4d, the nanofiber electrode delivers a discharge capacity of 1164 mA h g<sup>-1</sup> at 200 mA g<sup>-1</sup>, 973 mA h g<sup>-1</sup> at 400 mA g<sup>-1</sup>, 893 mA h g<sup>-1</sup> at 800 mA g<sup>-1</sup> and 745 mA h g<sup>-1</sup> at 2.0 A g<sup>-1</sup>. Even at very high rates of 3.0 A g<sup>-1</sup> and 4.0 A g<sup>-1</sup>, this electrode can still deliver considerably high reversible capacities of 676 mA h g<sup>-1</sup> and 616 mA h g<sup>-1</sup>, respectively. Once the current density returns to 200 mA g<sup>-1</sup> at the end of rate-cycling, the discharge capacity of the electrode recovers to 944 mA h g<sup>-1</sup> immediately, showing a strong tolerance for high current impact.

The above-presented results clearly demonstrate that the S/C/PAN nanofibers possess not only high capacity and long-term cyclability, but also excellent rate capability. Such superior performance may arise from their unique structural features: firstly, the sulfurized PAN matrix constitutes an electronically and ionically conducting framework that enable Li<sup>+</sup> ions and electrons to arrive at all the nanodomains in the electrode for the lithiation/delithiation reactions, thus ensuring a high utilization of the S/C composite. Secondly, the PAN matrix can separate the S/C nanoparticles from contact with electrolyte, considerably avoiding the side reaction between the reaction intermediates of sulfur and carbonate solvents and thus maintaining the activity of S/C composite during cycling. Finally, the linear structure and large length/diameter ratio of the S/C/PAN nanofibers allows the building of a network-like structure for the cathode, which can not only facilitate the ions transportation during cycling, but can also accommodate the mechanical stresses induced by volume changes of the cathode at repeated cycles, leading to an excellent rate and cycling performance. The structural stability is confirmed by the SEM image of the deeply cycled S/C/PAN nanofibers. As shown in Fig.S2, the nanofibers cycled over 400 cycles do not show any distinguishable change in their morphology and size distribution if compared to the uncycled nanofibers. Nevertheless, it should be pointed out that the sulfur content in the as-prepared nanofibers is not high compared with

the previously reported S/C composites that cycled in the ether-based electrolytes. To achieve high sulfur content, a microporous carbon matrix with highly developed surface area and porosity should be developed and used in this kind of composite. This work is under investigation in our Lab.

## Conclusions

In summary, we have successfully prepared S/C/PAN nanofibers using a single-nozzle electrospinning technique combined with a subsequent sulfurizing reaction. In the as prepared nanofibers, S/C nanoparticles are embedded homogeneously in the sulfurized PAN matrix to prevent their direct contact with liquid electrolyte, thus making this material electrochemically active in the carbonate-based electrolytes. The S/C/PAN nanofiber cathode in carbonate-based electrolyte shows almost 100% Coulombic efficiency and a capacity retention of ~ 730 mA h g<sup>-1</sup> over 400 cycles. These excellent electrochemical performances of the S/C/PAN nanofibers offer competitive advantages for constructing cycling-stable Li-S batteries. The novel structure and working mechanism of the S/C/PAN nanofibers may provide new insight into the design of long life and high capacity sulfur cathodes for practical development of Li-S batteries.

## Acknowledgements

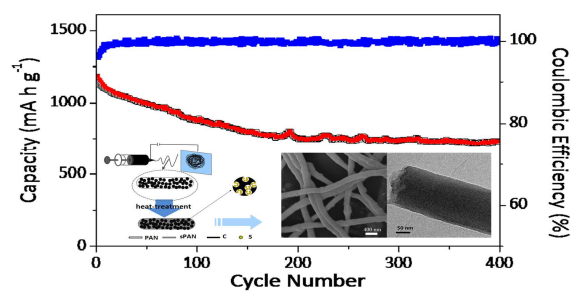
Financial supports from the National High-tech R&D Program of China (2012AA052201), the National Science Foundation of China (21373154) and the 973 Program (No. 2015CB251100) are greatly appreciated.

## Notes and references

- Hubei Key Lab. of Electrochemical Power Sources, College of Chemistry & Molecule science, Wuhan university, Wuhan, 430072, China. Fax: +86-27-87884476; Tel: +86-27-68754526; E-mail: xpai@whu.edu.cn*  
 † Electronic Supplementary Information (ESI) available: The cross-sectional-view SEM image and the corresponding elemental mapping of carbon and sulfur for the C/S/PAN nanofiber; SEM images of the C/S/PAN nanofiber electrode after 400 cycles. See DOI: 10.1039/b000000x/
- P. G. Bruce, S. A. Freunberger, L. J. Hardwick and J. M. Tarascon, *Nat. Mater.*, 2012, **11**, 19.
  - X.-P. Gao and H.-X. Yang, *Energy Environ. Sci.*, 2010, **3**, 174..
  - A. Manthiram, Y. Z. Fu and Y. S. Su, *Acc. Chem. Res.* 2013, **46**, 1125.
  - Y. Yang, G. Zheng and Y. Cui, *Chem. Soc. Rev.*, 2013, **42**, 3018-3032.
  - S. Evers and L. F. Nazar, *Acc. Chem. Res.*, 2013, **46**, 1135.
  - D. Bresser, S. Passerini and B. Scrosati, *Chem. Commun.*, 2013, **49**, 105457.
  - L. Chen and L. L. Shaw, *J. Power Sources*, 2014, **267**, 770.
  - W.H. Zhang, D. Qiao, J. X. Pan, Y. L. Cao, H. X. Yang and X. P. Ai, *Electrochim. Acta*, 2013, **87**, 497.
  - C. Huang, J. Xiao, Y. Shao, J. Zheng, W. D. Bennett, D. Lu, L. V. Saraf, M. Engelhard, L. Ji, J. Zhang, X. Li, G. L. Graff and J. Liu, *Nat. Commun.*, 2014, **5**, 3015.
  - S. Xin, L. Gu, N. H. Zhao, Y. X. Yin, L. J. Zhou, Y. G. Guo and L. J. Wan, *J. Am. Chem. Soc.* 2012, **134**, 18510.
  - J. Guo, Y. Xu and C. Wang, *Nano letters*, 2011, **11**, 4288.
  - V. S. Kolosnitsyn, E. V. Kuzmina and E. V. Karaseva, *J. Power Sources*, 2015, **274**, 203.
  - L. Sun, M. Li, Y. Jiang, W. Kong, K. Jiang, J. Wang and S. Fan, *Nano letters*, 2014, **14**, 4044.

14. R. Chen, T. Zhao, J. Lu, F. Wu, L. Li, J. Chen, G. Tan, Y. Ye and K. Amine, *Nano Lett.*, 2013, **13**, 4642.
15. Q. Li, Z. Zhang, Z. Guo, K. Zhang, Y. Lai and J. Li, *J. Power Sources*, 2015, **274**, 338.
16. S. Lu, Y. Cheng, X. Wu and J. Liu, *Nano Lett.*, 2013, **13**, 2485.
17. G. Zheng, Y. Yang, J. J. Cha, S. S. Hong and Y. Cui, *Nano Lett.*, 2011, **11**, 4462.
18. L. Ji, M. Rao, S. Aloni, L. Wang, E. J. Cairns and Y. Zhang, *Energy Environ. Sci.*, 2011, **4**, 5053
19. X. L. Ji, K. T. Lee, and L. F. Nazar, *Nat. Mater.*, 2009, **8**, 500.
20. B. Zhang, X. Qin, G. R. Li and X. P. Gao, *Energy Environ. Sci.*, 2010, **3**, 1531.
21. X. Liang, Z. Wen, Y. Liu, H. Zhang, L. Huang and J. Jin, *J. Power Sources*, 2011, **196**, 3655.
22. Z. Li, L. Yuan, Z. Yi, Y. Sun, Y. Liu, Y. Jiang, Y. Shen, Y. Xin, Z. Zhang and Y. Huang, *Adv. Energy Mater.*, 2014, **4**, 1301473
23. C. Zhao, L. Liu, H. Zhao, A. Krall, Z. Wen, J. Chen, P. Hurley, J. Jiang and Y. Li, *Nanoscale*, 2014, **6**, 882.
24. J. Song, T. Xu, M. L. Gordin, P. Zhu, D. Lv, Y. B. Jiang, Y. Chen, Y. Yuan and D. Wang, *Adv. Funct. Mater.*, 2014, **24**, 1243.
25. T. Xu, J. Song, M. L. Gordin, H. Sohn, Z. Yu, S. Chen and D. Wang, *ACS Appl. Mater. Interfaces*, 2013, **5**, 11355.
26. Q. Li, Z. Zhang, Z. Guo, Y. Lai, K. Zhang and J. Li, *Carbon*, 2014, **78**, 1.
27. S. Q. Chen, X. D. Huang, B. Sun, J. Q. Zhen, H. Liu, G. X. Wang, *J. Mater. Chem. A*, 2014, **2**, 161992.
28. Y. Chen, X. Li, K.-S. Park, J. Hong, J. Song, L. Zhou, Y.-W. Mai, H. Huang and J. B. Goodenough, *J. Mater. Chem. A*, 2014, **2**, 10126.
29. Z. Wang, S. Zhang, L. Zhang, R. Lin, X. Wu, H. Fang and Y. Ren, *J. Power Sources*, 2014, **248**, 337.
30. M. S. Park, J. S. Yu, K. J. Kim, G. Jeong, J. H. Kim, T. Yim, Y. N. Jo, U. Hwang, S. Kang, T. Woo, H. Kim and Y.-J. Kim, *RSC Adv.*, 2013, **3**, 11774.
31. J. T. Xu, J. L. Shui, J. L. Wang, M. Wang, H. K. Liu, S. X. Dou, I. Y. Deon, J. M. Seo, J. B. Beak and L. M. Dai, *ACS Nano*, 2014, **8**, 10920.
32. J. Zhang, Z. M. Dong, X. L. Dong, X. Y. Zhao, J. P. Tu, Q. M. Su, G. H. Du, *J. Power Sources*, 2014, **270**, 1.
33. Y. Qiu, W. Li, W. Zhao, G. Li, Y. Hou, M. Liu, L. Zhou, F. Ye, H. Li, Z. Wei, S. Yang, W. Duan, Y. Ye, J. Guo and Y. Zhang, *Nano Lett.*, 2014, **14**, 4821.
34. X. Ji, S. Evers, R. Black and L. F. Nazar, *Nat. Commun.*, 2011, **2**, 325.
35. X. Y. Liu, Z. Q. Shan, K. L. Zhu, J. Y. Du, Q. W. Tang, J. H. Tian, *J. Power Sources*, 2015, **274**, 85.
36. Z. Y. Zhang, Y. Q. Lai, Z. A. Zhang, K. Zhang, J. Li, *Electrochim. Acta*, 2014, **129**, 55.
37. H. B. Yao, K. Yan, W. Y. Li, G. Y. Zheng, D. S. Kong, Z. W. Seh, V. K. Narasimhan, Z. Liang, Y. Cui, *Energy Environ. Sci.*, 2014, **7**, 3381.
38. S. Chen, F. Dai, M. L. Gordin and D. Wang, *RSC Advances*, 2013, **3**, 3540.
39. M. L. Gordin, F. Dai, S. Chen, T. Xu, J. Song, D. Tang, N. Azimi, Z. Zhang and D. Wang, *ACS Appl. Mater. Interfaces*, 2014, **6**, 8006.
40. N. Azimi, W. Weng, C. Takoudis and Z. Zhang, *Electrochem. Commun.*, 2013, **37**, 96.
41. S. Kinoshita, K. Okuda, N. Machida and T. Shigematsu, *J. Power Sources*, 2014, **269**, 727.
42. L. Suo, Y. S. Hu, H. Li, M. Armand and L. Chen, *Nat. Commun.*, 2013, **4**, 1481.
43. S. S. Zhang, *Electrochim. Acta*, 2012, **70**, 344.
44. Z. Lin, Z. Liu, W. Fu, N. J. Dudney and C. Liang, *Adv. Funct. Mater.*, 2013, **23**, 1064.
45. F. Wu, S. Wu, R. Chen, J. Chen and S. Chen, *Electrochem. Solid - State Lett.*, 2010, **13**, A29.
46. Z. Dong, J. Zhang, X. Zhao, J. Tu, Q. Su and G. Du, *RSC Adv.*, 2013, **3**, 24914.
47. L. Xiao, Y. Cao, J. Xiao, B. Schwenzer, M. H. Engelhard, L. V. Saraf, Z. Nie, G. J. Exarhos and J. Liu, *Adv. Mat.*, 2012, **24**, 1176.
48. J. Fanous, M. Wegner, J. Grimming, A. Andresen and M. R. Buchmeiser, *Chem. Mater.*, 2011, **23**, 5024.
49. Z. Wang, Y. Dong, H. Li, Z. Zhao, H. B. Wu, C. Hao, S. Liu, J. Qiu and X. W. Lou, *Nat. Commun.*, 2014, **5**, 5002.
50. Y. Z. Zhang, S. Liu, G. C. Li, G. R. Li and X. P. Gao, *J. Mater. Chem. A*, 2014, **2**, 4652.
51. T. N. L. Doan, M. Ghaznavi, A. Konarov, Y. Zhang and P. Chen, *J. Solid State Electrochem.*, 2013, **18**, 69.

## Graphical Abstract



A cycling-stable sulfur electrode in carbonated-based electrolytes is developed by embedding S/C nanoparticles in the PAN-based nanofibers.